STRATOSPHERE AND MESOSPHERE DENSITY-HEIGHT PROFILES OBTAINED WITH THE X-15 AIRPLANE

Earl J. Montoya and Terry J. Larson

NASA Flight Research Center, Edwards, California

Abstract. Density-height profiles in the stratosphere and mesosphere were obtained from impact-pressure, velocity, and altitude measurements made on six X-15 research airplane flights. A form of the Rayleigh pitot formula was used for density computations. Because of pressure-instrumentation limitations and pressure lag, the maximum altitude for reasonably accurate density determination was considered to be about 65 km. Good agreement was obtained between temperatures calculated from faired density-height profiles of two X-15 flights and temperatures measured by rocketsondes launched near the times of flight from the Pacific Missile Range, Point Mugu, California.

(H-352)

STRATOSPHERE AND MESOSPHERE DENSITY-HEIGHT PROFILES OBTAINED WITH THE X-15 AIRPLANE

Earl J. Montoya and Terry J. Larson

NASA Flight Research Center, Edwards, California

INTRODUCTION

The X-15 research program provides an opportunity to obtain atmospheric data in the stratosphere and the mesosphere by virtue of both the high altitudes obtained by the X-15 airplane (Figure 1) and the research instrumentation installed in support of the basic research program. Analysis showed that, with the particular instrumentation available, density could be determined more accurately than temperature or pressure. The calculation technique selected is based on a form of the Rayleigh pitot equation similar to that used by Ainsworth, et al. [1961] for the continuum-flow regions of an Aerobee flight launched from Fort Churchill, Canada, in 1958. This method requires only impact pressure, velocity, and altitude measurements at high supersonic speeds and is, thus, particularly applicable to X-15 data, inasmuch as the X-15 impact-pressure measurements are not subject to flow angularity effects.

A number of density profiles were determined. Six of these profiles, from flights made over Southern California and Nevada between March 30, 1961, and August 22, 1963, are presented and discussed in this paper. The profiles are significant in that they (1) add to the atmospheric data in the altitude range not covered by radiosonde balloons and satellite measurements and only recently being extensively explored by the Meteorological Rocket Network, and they (2) demonstrate the applicability of impact-pressure measurements from flight vehicles in the determination of atmospheric density.

METHODS AND MEASUREMENTS

For continuum-flow conditions at supersonic speeds, atmospheric density may be obtained from a modified form of the Rayleigh pitot equation (see Appendix for derivation)

$$\rho^3 - \frac{1.086}{V^2}\rho^2(p_t - 0.460p) + \frac{0.175p^2}{V^4}\rho + 0.0525\frac{p^3}{V^6} \approx 0$$

where ρ = density, p = ambient pressure, p_t = impact pressure, and V = velocity. The constants in this equation were evaluated, using a specific-heat ratio of 1.4 for air. Although the terms which include static pressure are relatively insignificant at the high Mach numbers (greater than 2.5) associated with the data of this paper, the preceding five-term equation was programed to obtain maximum accuracy for density determination over the entire supersonic Mach number range of the X-15.

Impact-pressure measurements were obtained from the stagnation port of the X-15 airflow sensor, commonly referred to as the ball nose (Figure 2). The sensor has a pressure-nulling type of servomechanism which constantly orients the stagnation port toward the local airstream. Thus, the measurement of impact pressure is not subject to flow angularity effects as are pressure measurements from some sounding rockets.

Ambient-pressure measurements were obtained up to altitudes of 30 km from rawinsonde balloons released at Edwards, California, by the Air Weather Service. At the higher altitudes (for which rawinsonde data were unavailable), values from the U.S. Standard Atmosphere, 1962, were used. As previously mentioned, however, accurate determination of static pressure is not critical for the data of this paper.

Velocity and altitude measurements were obtained from three AFMTC-Mod II radars (modified SCR-584 radars). Usually, simultaneous data were available

from two radars, although computations of velocity and altitude were based on a single-station solution. Fairings were made by subjective analysis. True air velocity was computed by vector addition of wind velocity and radar-determined velocity. The wind velocity was acquired either from AN/GMD-1 rawinsonde measurements or from sounding-rocket measurements from the Pacific Missile Range, Pt. Mugu, California (fig 3). TO TIE IN WITH FIG 3

Measurements were obtained on two of the three X-15 aircraft, the X-15-2 and the X-15-3. On the two density-data flights of the X-15-2, impact pressures were not recorded directly but were obtained from a static-pressure measurement and a differential-pressure measurement. Static pressure was measured from the fuselage manifolded orifices and differential pressure from the static source and the stagnation port of the ball nose. These two measurements, when summed, gave the required impact pressure.

Impact pressures were obtained similarly for X-15-3 data flights at altitudes below 40 km. Above this altitude, however, impact pressures were recorded directly by standard NACA airspeed-altitude recorders, which are mechanical-optical instruments using both absolute and differential cells. Table 1 lists the altitude ranges of the cells.

LIMITATIONS AND ACCURACY

For the X-15 flight conditions, real-gas effects on the validity of the Rayleigh pitot equation are insignificant. Therefore, no attempts were made to correct for deviations from the ideal-gas relations or for minor ionization effects that occur in the speed range where the measurements were made. The effects of the variation of specific-heat ratio for air (caloric effects) were also considered. By using a specific heat ratio of 1.4, it was found that density errors were less than 1 per cent for the X-15 flight conditions encountered; thus, no caloric corrections were made.

According to Kane and Maslach [1950] and Sherman [1953], corrections to impact pressures are necessary when the Rayleigh pitot equation is used for compressible flow conditions associated with viscous forces that are significant in comparison to the inertia or pressure forces in the fluid. Data from these studies indicate that corrections for viscous effects are appropriate when free-stream Reynolds numbers are less than about 300 for impact-pressure installations similar to those of the X-15 airflow sensor. For the 1.27-cm-diameter orifice of the sensor and the X-15 flight velocities encountered, Reynolds numbers below 300 are limited to altitudes greater than about 60 km. Since the basic measurement errors are, evidently, considerably larger than the indicated viscous corrections for the pertinent flight conditions, no corrections for viscosity have been applied. Because of the probable inaccuracies in the pressure data and in space positioning, the density profiles presented are smoothed density-variation curves and do not portray small-scale details of the atmospheric soundings.

Of primary importance in obtaining the derived density is the measurement of impact pressure. Meaningful density data have been determined to altitudes of approximately 65 km by means of pressure recorders routinely installed on research aircraft at the NASA Flight Research Center. The cells of these recorders are accurate from 0.25 per cent to about 0.50 per cent of full-scale range. For the extreme flight conditions encountered with the X-15, the latter value was used for the estimation of density errors shown in Table 2. The recorded pressures for the portions of flights that had simultaneous recordings of either two absolute or two differential cells of different ranges indicate disagreements significantly less than 0.50 per cent of the higher range cells.

Because of space limitations behind the impact port of the ball nose, longer tubing (60 cm) than desired was required between the impact-pressure port and the recorder. As a result of the large impact opening (1.27 cm), the

large-bore tubing (0.75 cm minimum), and the small instrument volumes, however, the associated pressure lag was relatively small up to an altitude of 61 km.

Inasmuch as the individual errors listed in Table 2 are maximum errors and are independent, a 3σ error is included to represent the overall maximum probable density error. Although it is not likely that the individual errors are additive, the fact that the maximum error due to impact-pressure measurement is about an order of magnitude larger than any of the other errors lessens the probability of significant compensation at the higher levels of measurement. In addition to the density errors, it is estimated that maximum altitude errors are 0.3 km.

PRESENTATION AND ANALYSIS OF DATA

The geographical location of the area (shaded) over which the measurements presented herein were obtained is shown in Figure 3. A time history of the pertinent flight quantities (impact pressure p_t, velocity V, and altitude h) is presented in Figure 4 to indicate the approximate range and variation of these quantities for a typical X-15 flight.

The variation of density with altitude, as determined by measurements obtained on six X-15 flights, is shown in Figures 5 through 10. The data for the two X-15-2 flights (Figures 5 and 6) are not considered to be as accurate at altitudes above about 40 km as those of the X-15-3 flights (Figures 7 to 10) because of the less sensitive pressure cells on the X-15-2. A distinction is made between the ascent and descent portions of the flights to aid in interpreting the data. Also shown are density values obtained from rawinsonde measurements (at the lower altitudes) and the U.S. Standard Atmosphere, 1962.

At altitudes below 61 km for which lag effects should be insignificant, the difference between ascent and descent points measures the repeatability of the data for a given altitude and flight. Below 65 km, the average scatter is

approximately ±5 per cent. From Table 2 it is evident that scatter between ascent and descent points for altitudes less than approximately 50 km reflects, primarily, velocity and altitude errors rather than pressure errors. At these altitudes, therefore, the density-height fairings have been made to correspond more closely to the points calculated from the radar data considered to be the most accurate. Also, more weight was given to the rawinsonde densities (where available), inasmuch as they are regarded as generally the most accurate of the data presented.

At altitudes in excess of 65 km, the ascent and descent points diverge with altitude. This divergence is caused primarily by lag in the pressure-measuring system, as indicated by the consistently higher ascent than descent impact pressures at comparable altitudes. Because of this lag effect, as well as the known limitations of the impact-pressure measurements and viscous effects at high altitudes, meaningful density data for any of the flights cannot be expected at altitudes above 65 km.

The validity of the faired density-height profiles at altitudes where meaningful data can be expected was indirectly confirmed by data obtained from two Arcas rocketsondes launched from the Pacific Missile Range near the times of two X-15-3 flights. Temperatures calculated from the density-height profiles of Figures 9 and 10 are compared in Figures 11 and 12, respectively, with temperatures measured by the Arcas 10-mil bead thermistor.

Densities were converted to temperatures by using the equation

$$T_2 = \frac{\rho_1 M_2}{\rho_2 M_1}\left(T_1 - \frac{M_1}{\rho_1 R}\int_{h_1}^{h_2} \rho g dh\right)$$

where M is the molecular weight, R is the gas constant, g is the acceleration of gravity, and dh is the differential of altitude. The subscripts refer to the end points of the considered altitude interval. By using the

temperature given by the U.S. Standard Atmosphere, 1962, at 61 km and the densities from the curves of Figures 9 and 10 for this altitude, temperatures were calculated for progressively lower altitudes in intervals of 0.61 km for each flight. A constant value of molecular weight (M = 28.9 for air) was used. As pointed out by Ainsworth et al. [1961], an error in the initial choice of temperature becomes relatively insignificant after integration over a number of kilometers of altitude.

The Arcas temperature data were corrected for radiation effects as suggested by Wagner [1963]. The small differences between Arcas and X-15 temperatures (Figures 11 and 12) indicate good agreement, considering the possible errors in the Arcas temperature measurements (±2 per cent with Wagner's corrections) and the horizontal separation (maximum of about 375 km) between the two sets of data.

In Figures 5 through 10, the density-height profiles consistently indicate higher densities than the standard values above altitudes from about 35 km to 45 km. Figure 10 indicates a possible crossover point at altitudes in excess of approximately 60 km. As shown, the differences between the flight data and the Standard Atmosphere generally vary consistently from about 5 to 7 per cent over large altitude ranges. This consistency adds further validity to the density-height fairings and the usefulness of the measurements made with the X-15 airplane.

65-66 km?

APPENDIX

DERIVATION OF ATMOSPHERIC DENSITY FROM RAYLEIGH PITOT EQUATION

The relationship between stagnation pressure p_t measured behind a normal shock, free-stream static pressure p, and free-stream supersonic Mach number M is given by the Rayleigh pitot equation

$$\frac{p_t}{p} = \left[\frac{(\gamma + 1)}{2}\right]^{\frac{\gamma+1}{\gamma-1}} \gamma^{-\frac{1}{\gamma-1}} M^2 \left[1 - \frac{(\gamma - 1)}{2\gamma M^2}\right]^{-\frac{1}{\gamma-1}}$$

where γ is the specific-heat ratio for the gas. Proceeding as outlined by Newell [1953], $\frac{\gamma p}{\rho}$ may be substituted for a^2 (speed of sound) so that $M^2 = \frac{\rho V^2}{\gamma p}$. Substituting this expression into the Rayleigh pitot equation and expanding

$$\frac{p_t}{p} = \frac{B\rho V^2}{\gamma p}\left[1 - \frac{p}{2\rho V^2} + \frac{\gamma p^2}{8\rho^2 V^4} + \frac{\gamma(2\gamma - 1)p^3}{48\rho^3 V^6} + \cdots\right]$$

where

$$B = \left[\frac{(\gamma + 1)}{2}\right]^{\frac{\gamma+1}{\gamma-1}} \gamma^{-\frac{\gamma}{\gamma-1}}$$

which may be expressed as the cubic

$$\rho^3 - \frac{\rho^2}{BV^2}\left(p_t - \frac{Bp}{2}\right) + \frac{\gamma p^2 \rho}{8V^4} + \frac{\gamma(2\gamma - 1)}{48V^6} p^3 \approx 0$$

By choosing $\gamma = 1.4$ for air, the derived equation becomes

$$\rho^3 - \frac{1.086}{V^2}\rho^2(p_t - 0.4605p) + \frac{0.175p^2\rho}{V^4} + \frac{0.0525p^3}{V^6} \approx 0$$

Acknowledgements. We thank Pacific Missile Range personnel for sounding-rocket data obtained in support of the X-15 program and appreciate the coordination by the NASA Pacific Launch Operations Office. We also wish to express our appreciation to Detachment 21 of the 4th Weather Group, Edwards Air Force Base, for providing rawinsonde data for X-15 flights and for their general assistance. We would like to acknowledge, too, the contributions of Mr. Harold P. Washington of the NASA Flight Research Center.

REFERENCES

Ainsworth, J. E., D. F. Fox, and H. E. LaGow, Measurement of upper-atmosphere structure by means of the pitot-static tube, NASA Tech. Note D-670, 1961.

Kane, E. D. and G. J. Maslach, Impact-pressure interpretation in a rarefied gas at supersonic speeds, NACA Tech. Note 2210, 1950.

Sherman, F. S., New experiments on impact-pressure interpretation in supersonic and subsonic rarefied air streams, NACA Tech. Note 2995, 1953.

Duberg, J. E., W. J. O'Sullivan, Jr., R. A. Hord, S. L. Seaton, J. A. Mullins, et al., U.S. Standard Atmosphere, 1962, U.S. Government Printing Office, Washington, D. C., Dec. 1962.

Wagner, N. K., Theoretical accuracy of the meteorological rocketsonde thermistor, Rept 7-23, Electrical Engineering Research Laboratory, University of Texas, p. 32, 1 July 1963.

Newell, Homer E., Jr., High altitude rocket research, pp. 121-124, Academic Press, New York, 1953.

TABLE 1. Pressure-Measurement Cell Ranges

Airplane	Range		
	Altitude, km	Absolute cell, mm Hg	Differential cell, mm Hg
X-15-2	16—26	0—790	0—940
	26—38	0—30	0—940
	38—66	0—30	0—90
X-15-3	18—40	0—800	0—940
	40—74	0—40	Not required

TABLE 2. Estimation of Density Errors

Altitude, km	Density errors, %					
	Velocity	p	p_t	Lag	γ	Max. probable error†
30.5	5.2	Negligible	2.4	Negligible	0.75	5.8
45.6	7.5	2.0	2.5(6.8)*	Negligible	0.75	8.2(10.4)*
61.0	2.6	2.5	11.2(28.0)*	1.0	0.75	11.8(28.3)*

*X-15-2 only.
†3σ (root sum square).

NASA

E-7469

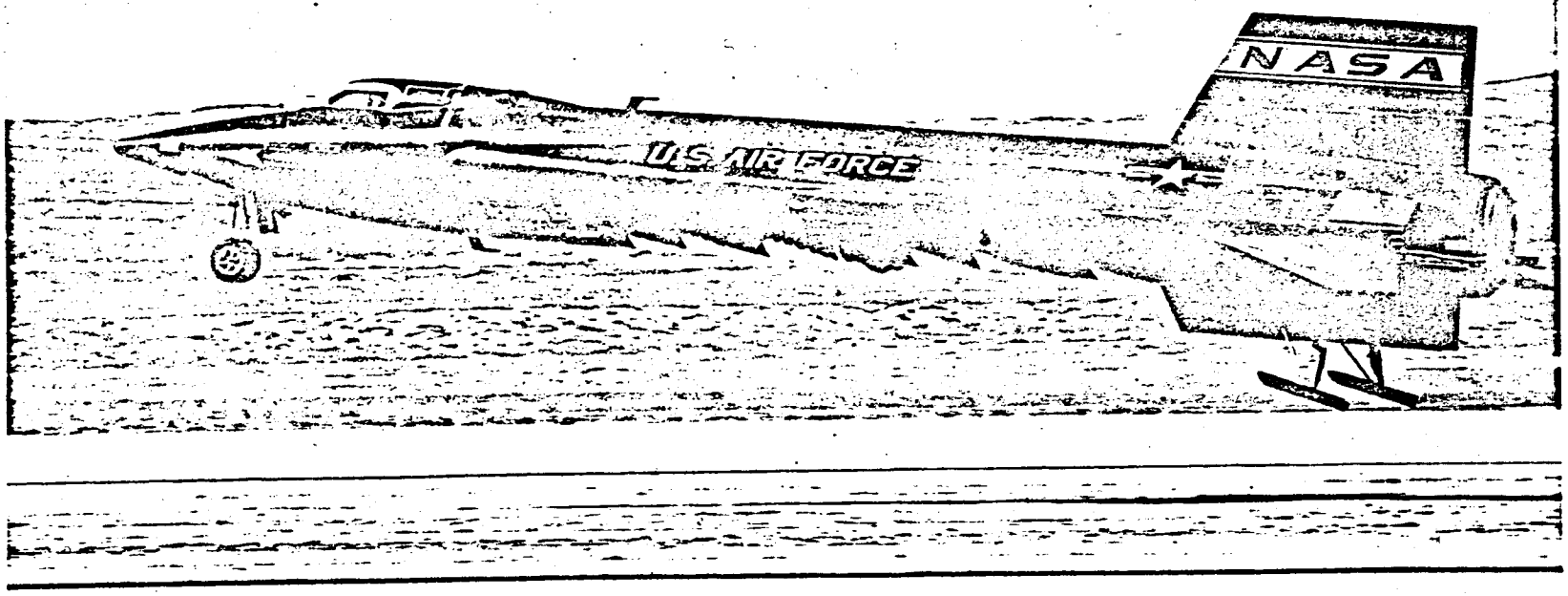

Fig. 1. X-15 airplane in the landing configuration.

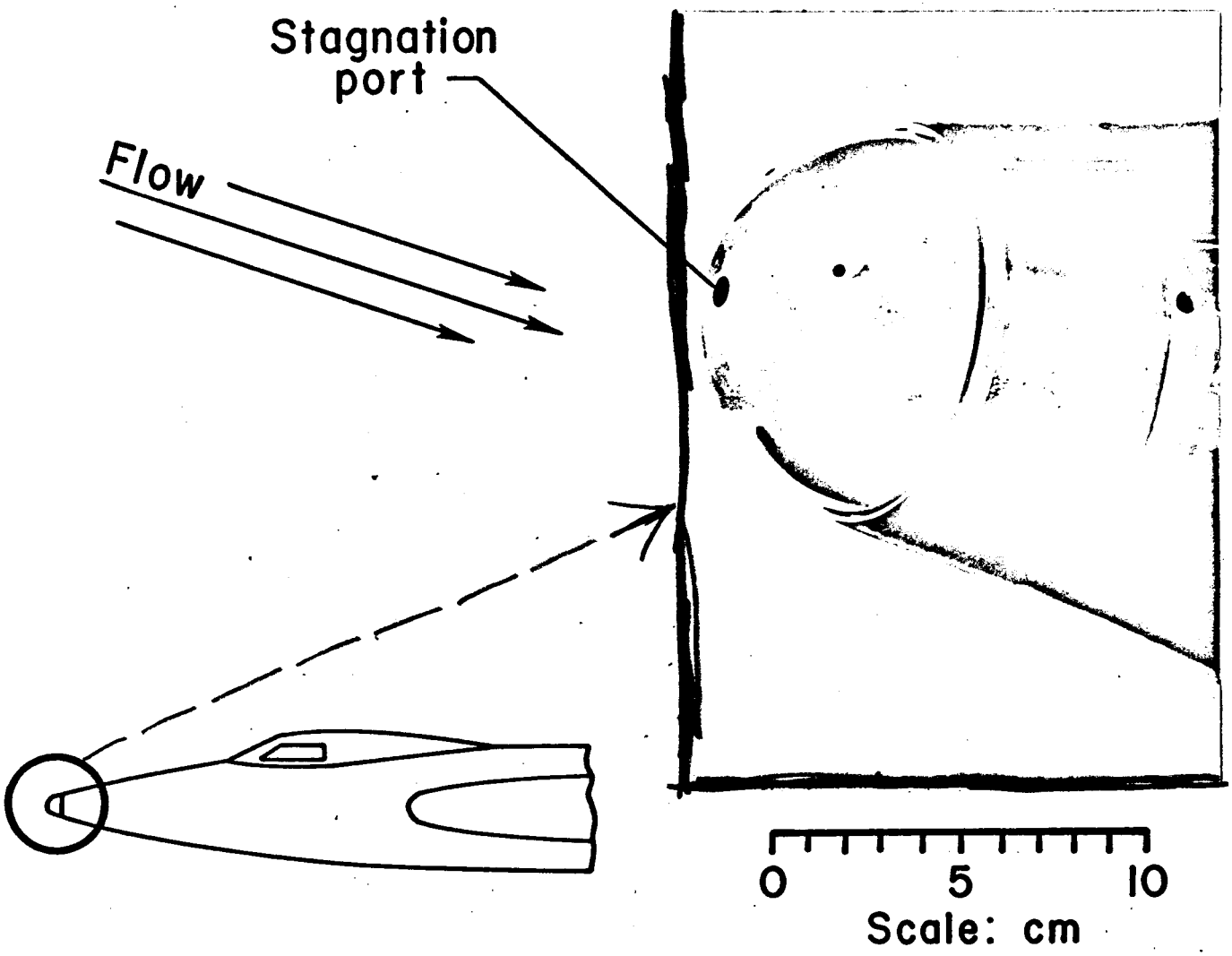

Fig. 2. X-15 flow-direction sensor (ball nose).

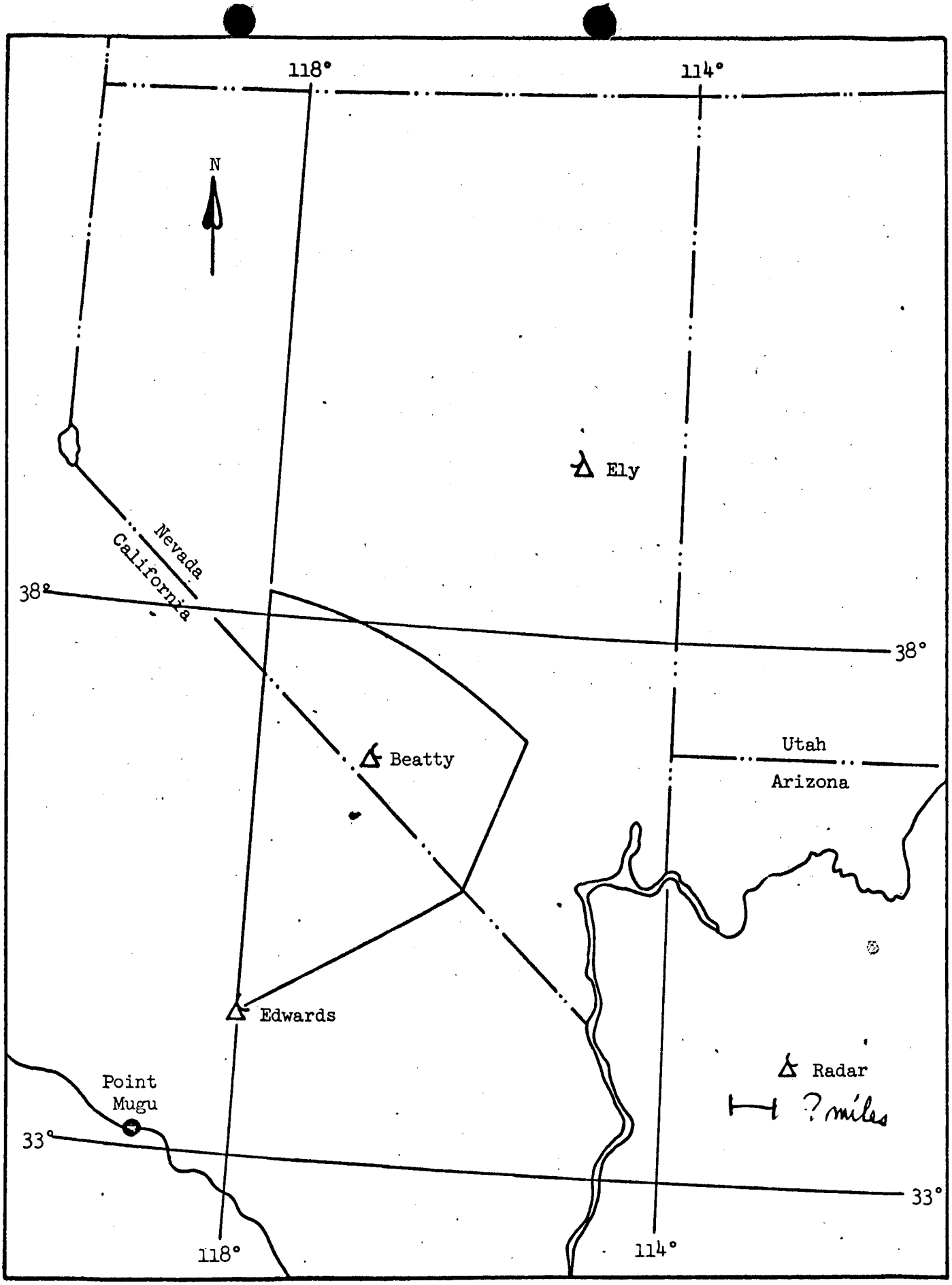

Fig. 3. Geographical area over which X-15 density measurements were made.

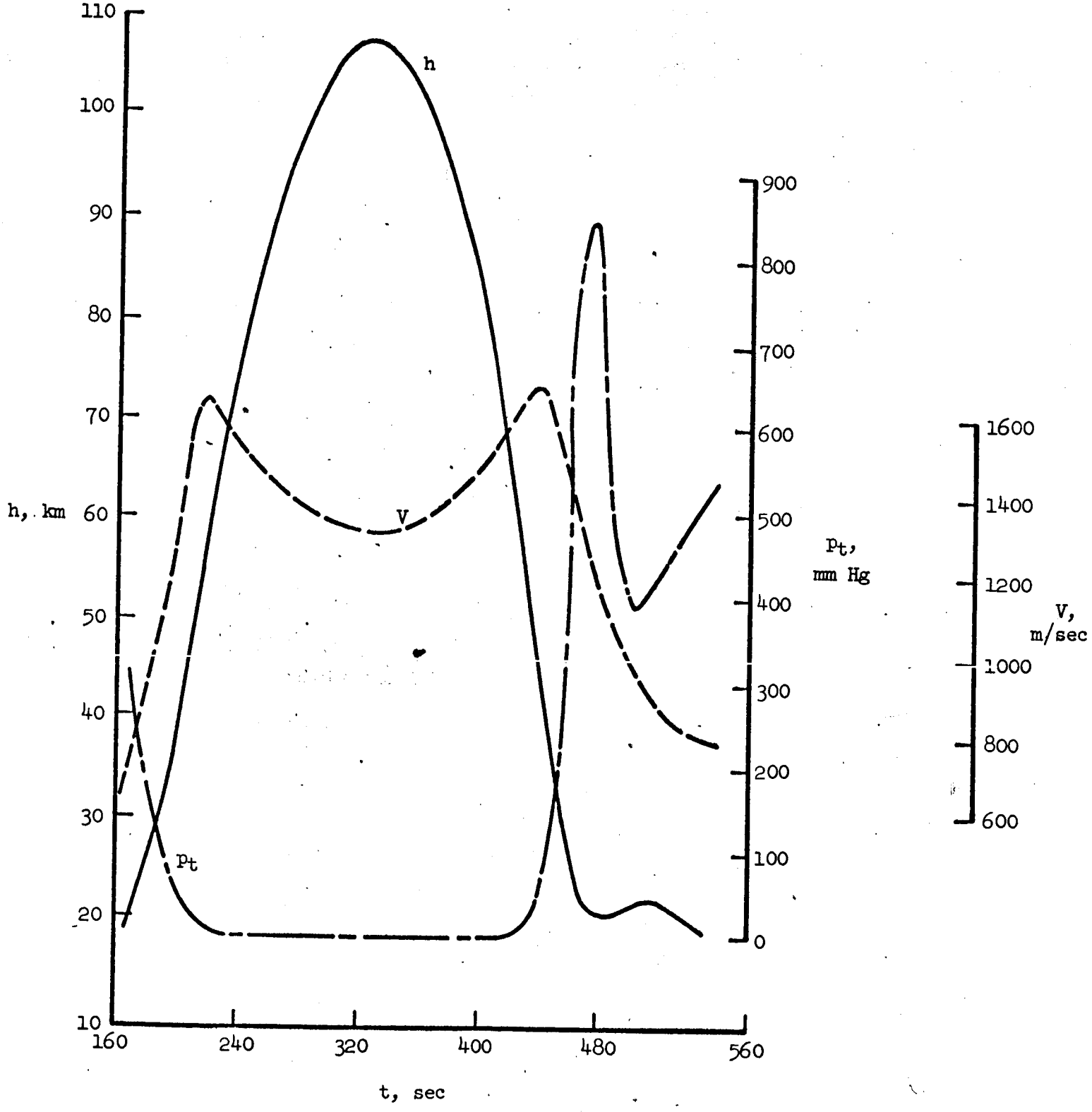

Fig. 4. Typical X-15 time history of pertinent quantities required for density determination.

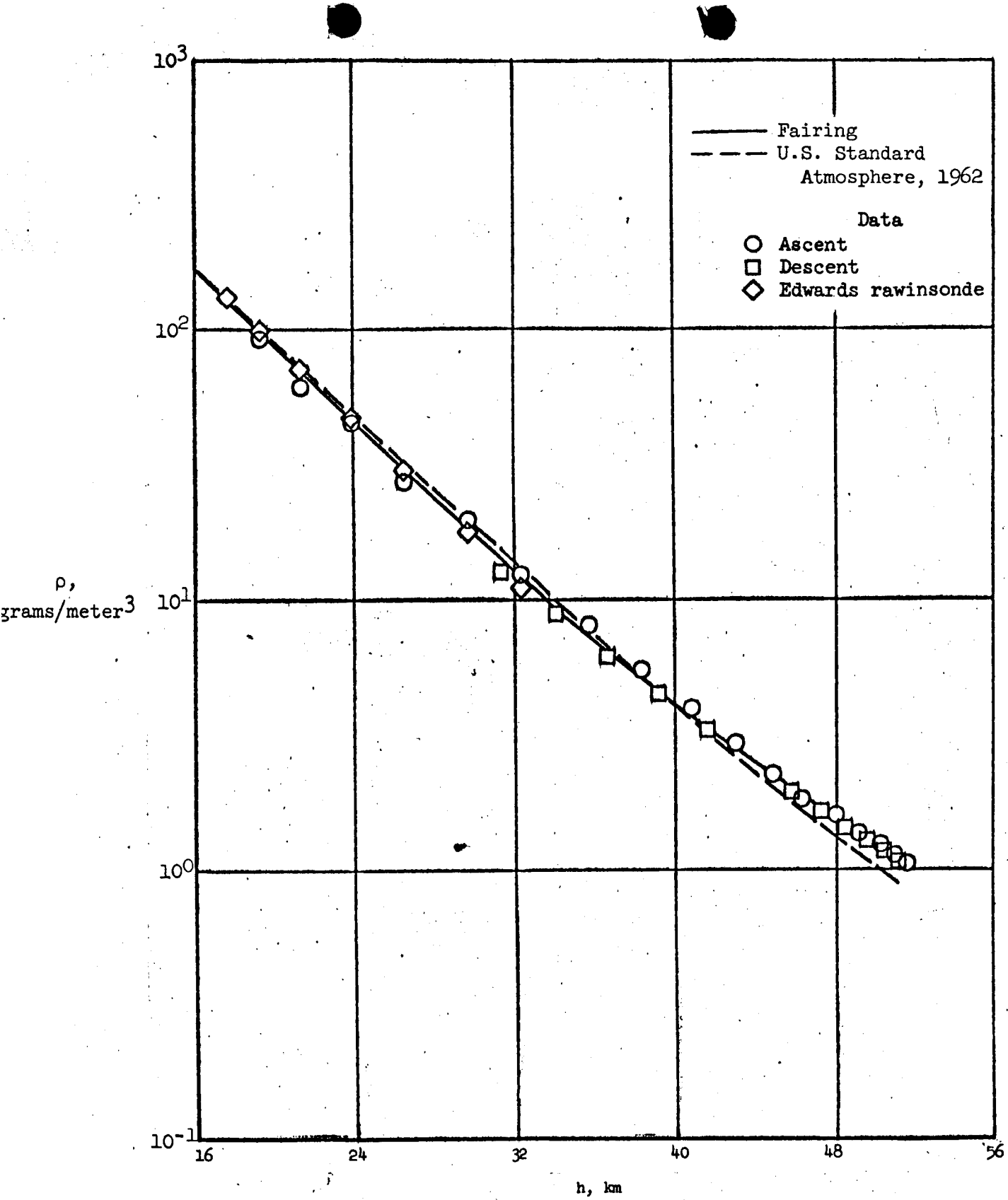

Fig. 5. Atmospheric-density-height profile determined from X-15-2 flight on March 30, 1961.

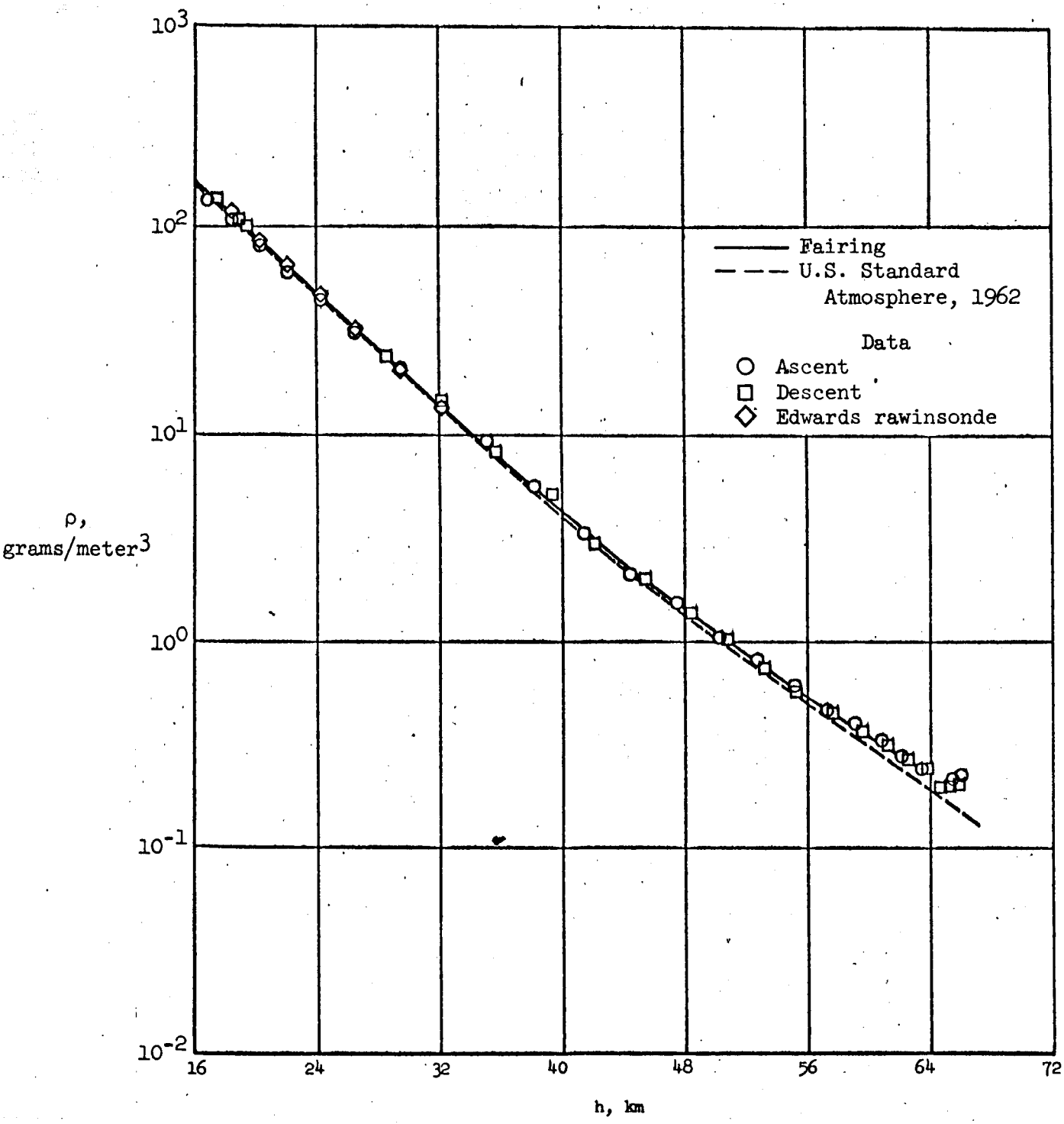

Fig. 6. Atmospheric-density-height profile determined from X-15-2 flight on October 11, 1961.

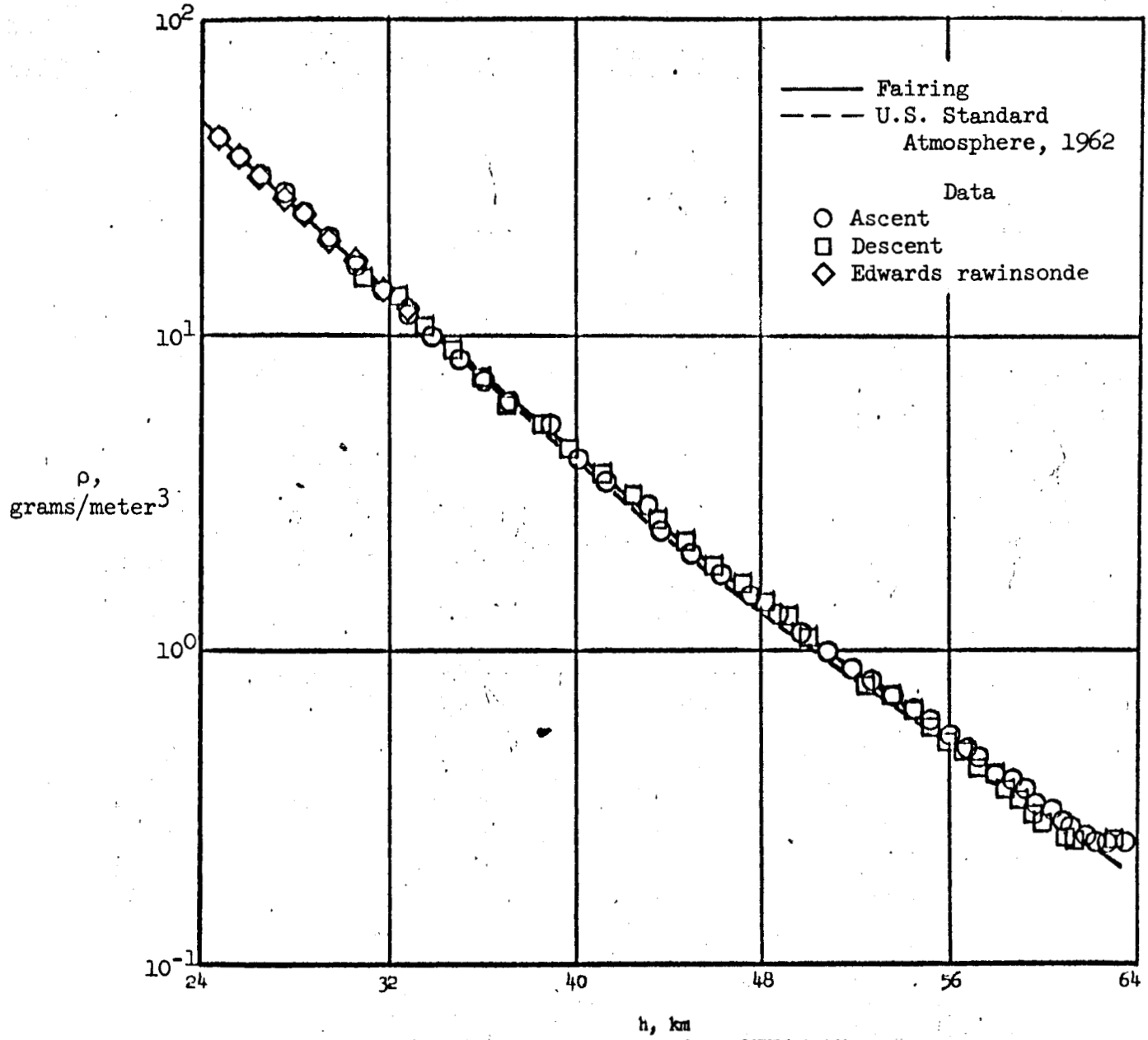

Fig. 7. Atmospheric-density-height profile determined from X-15-3 flight on May 2, 1963.

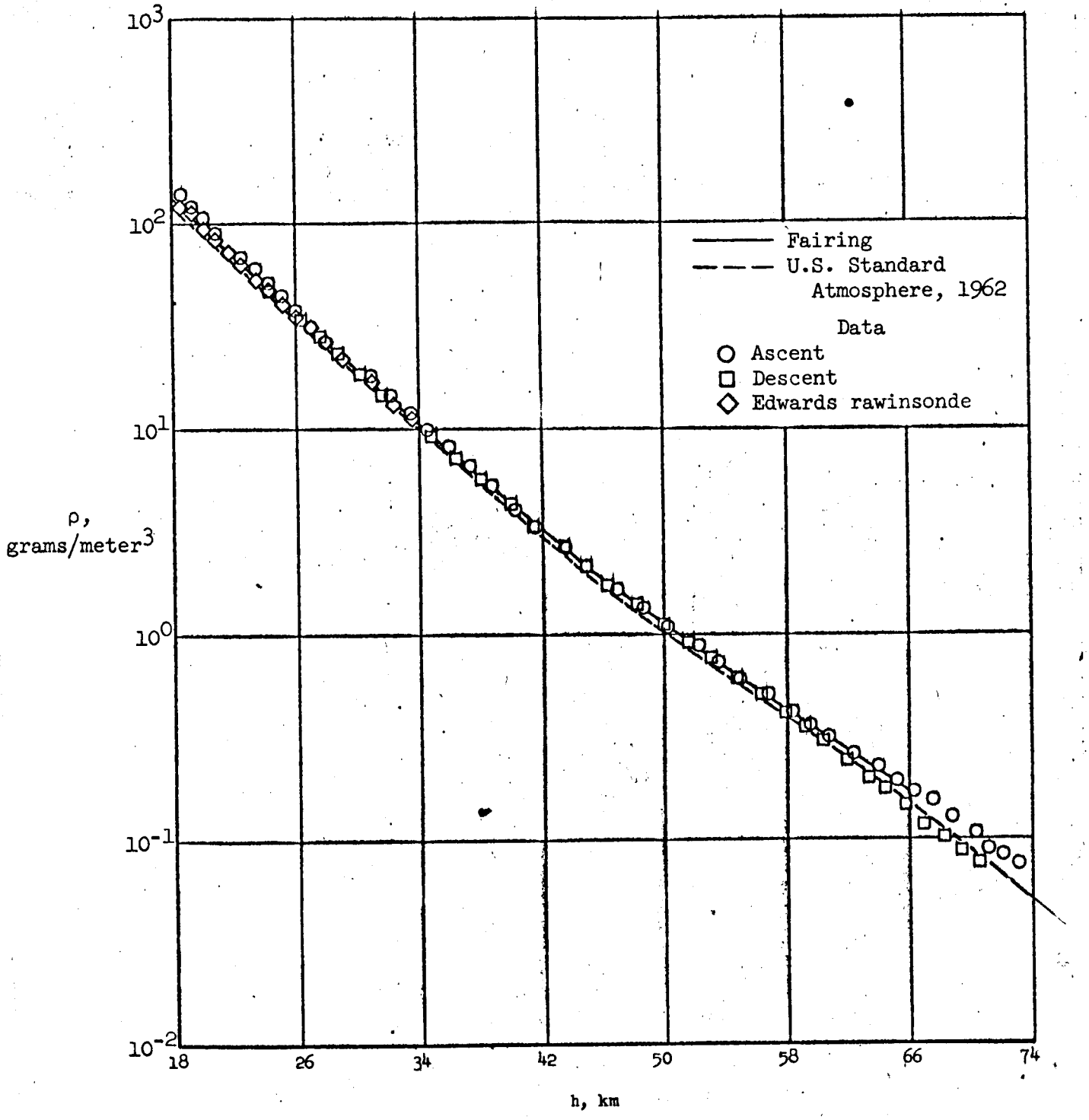

Fig. 8. Atmospheric-density-height profile determined from X-15-3 flight on June 27, 1963.

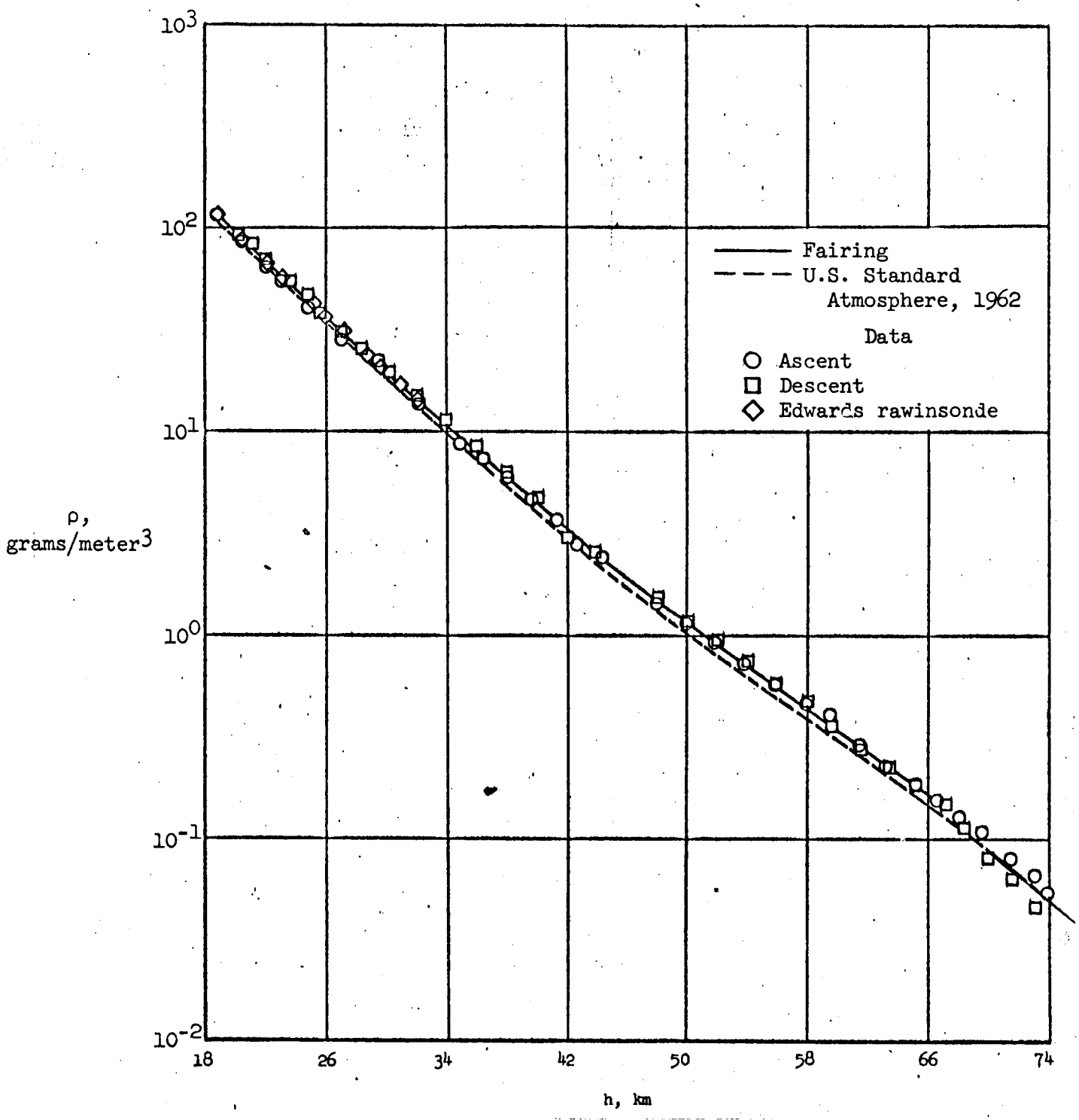

Fig. 9. Atmospheric-density-height profile determined from X-15-3 flight on July 19, 1963.

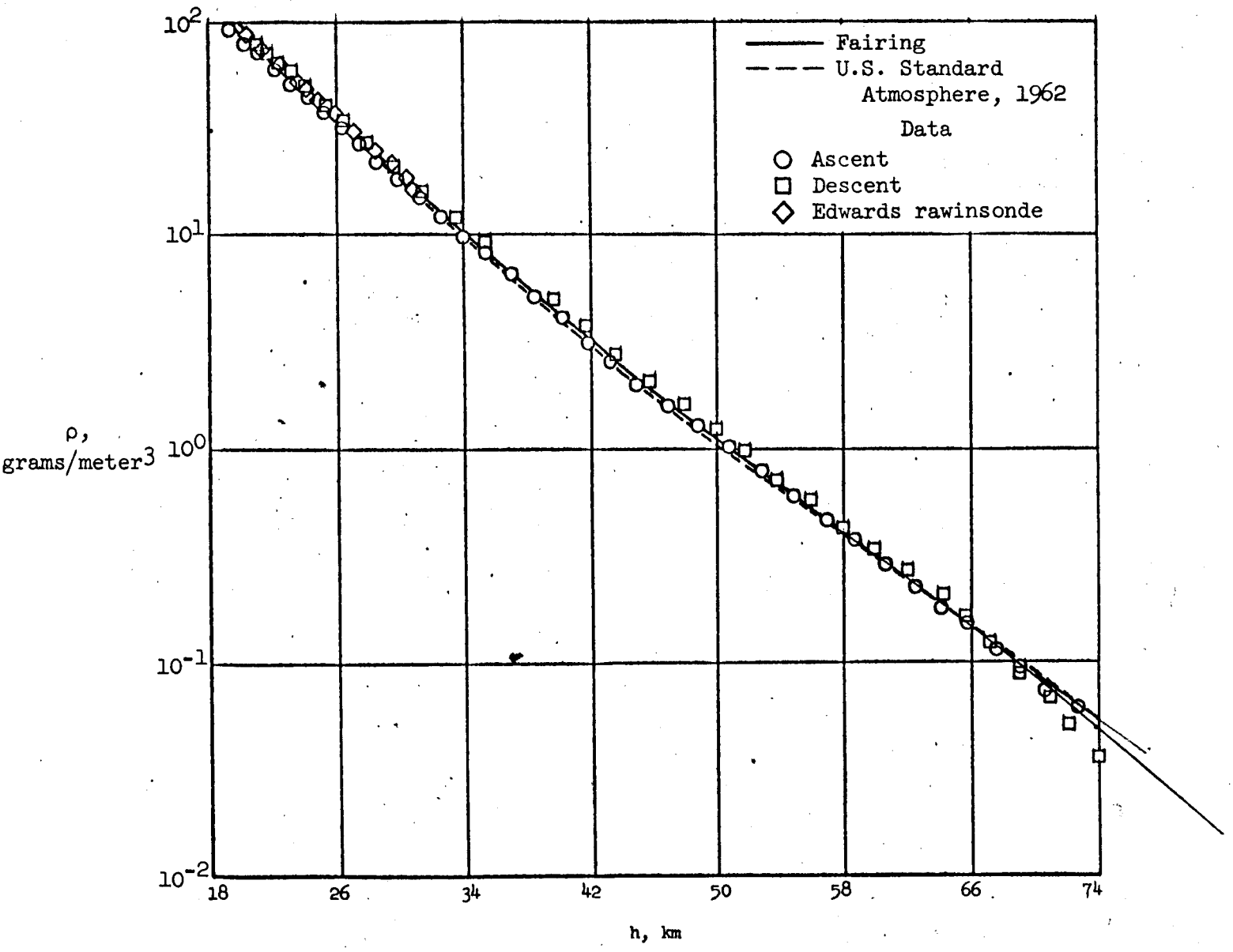

Fig. 10. Atmospheric-density-height profile determined from X-15-3 flight on August 22, 1963.

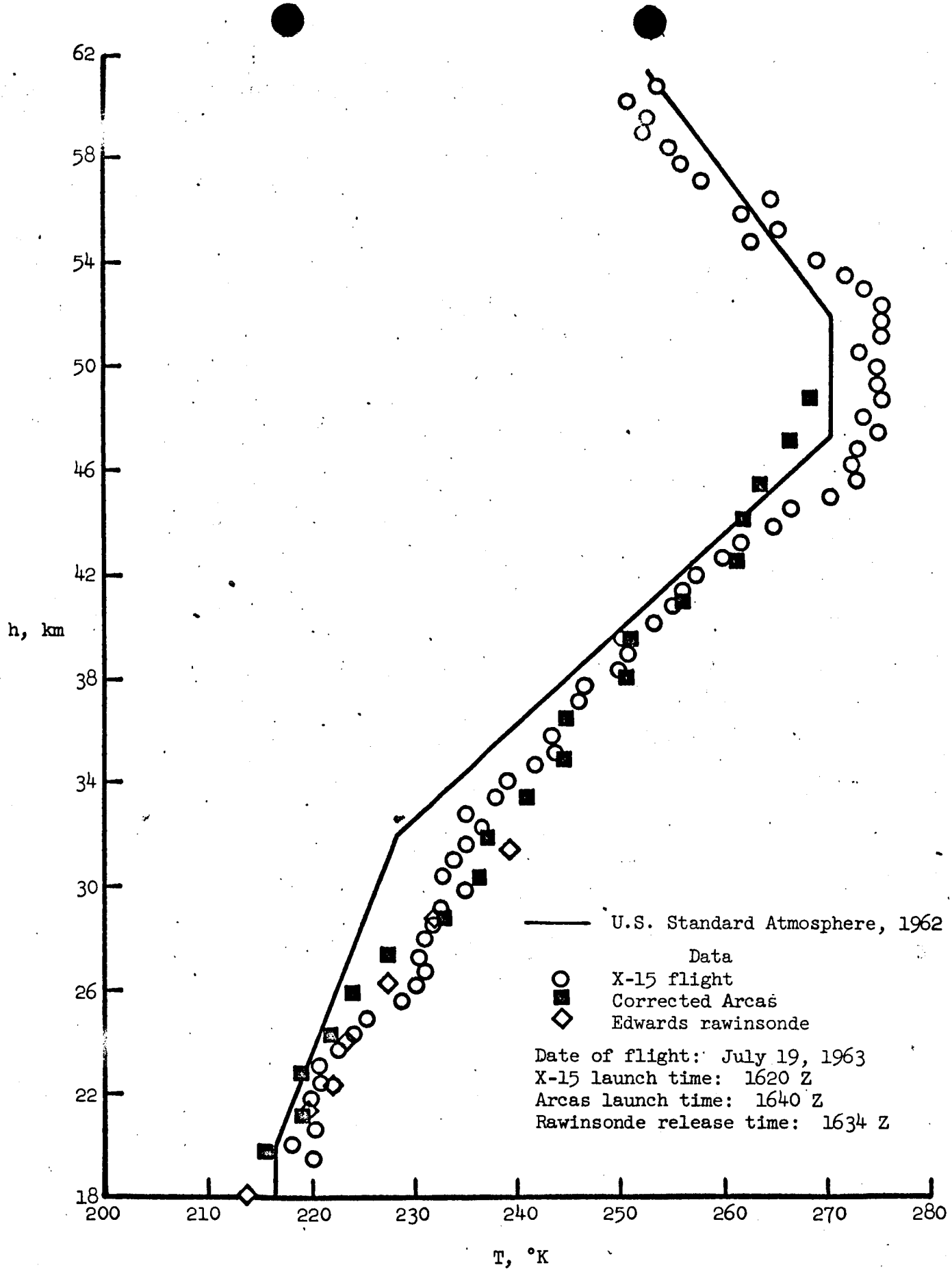

Fig. 11. Comparison of temperatures calculated from density-height profile of figure 9 with Arcas rocketsonde temperatures.

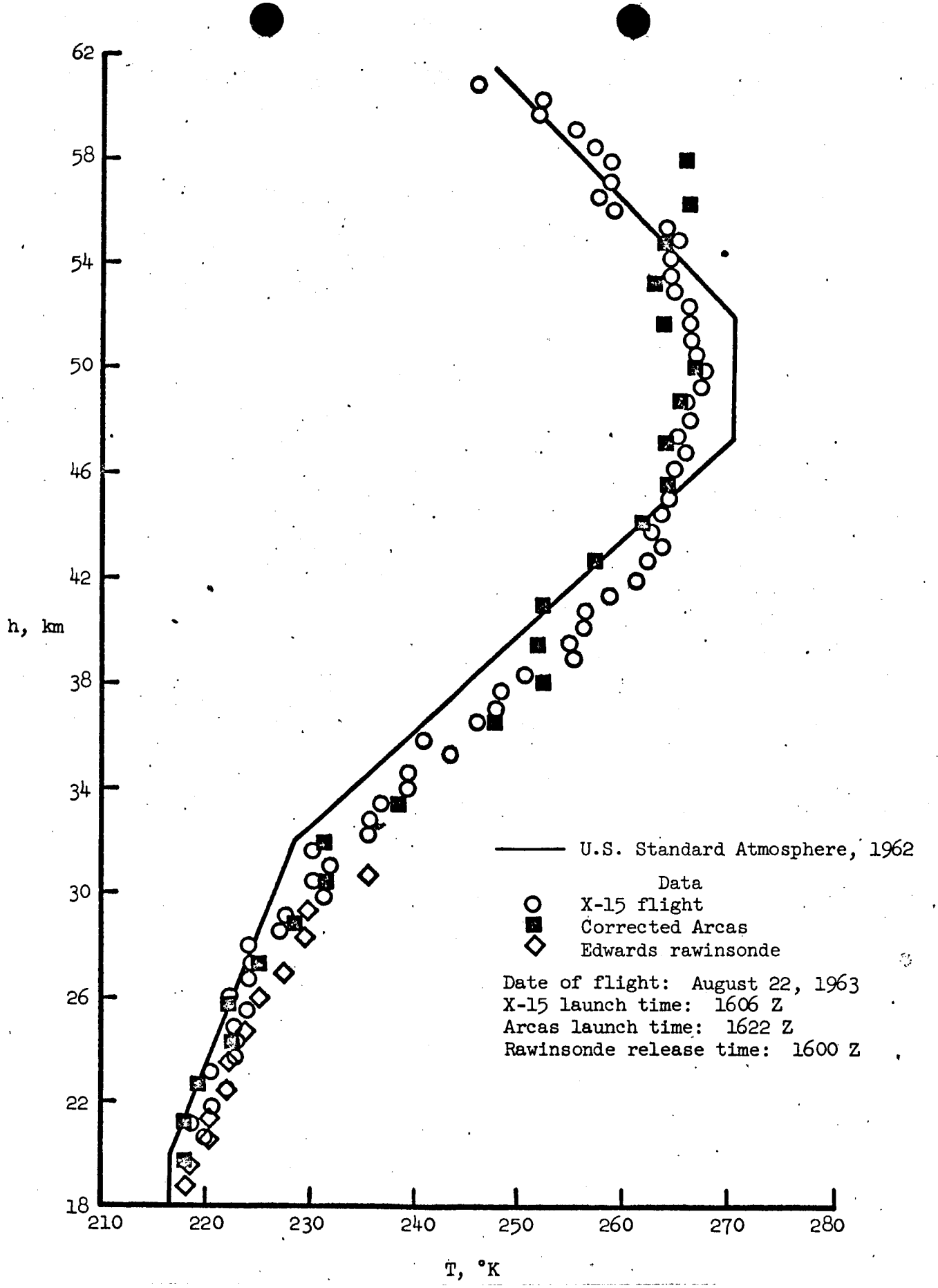

Fig. 12. Comparison of temperatures calculated from density-height profile of figure 10 with Arcas rocketsonde temperatures.

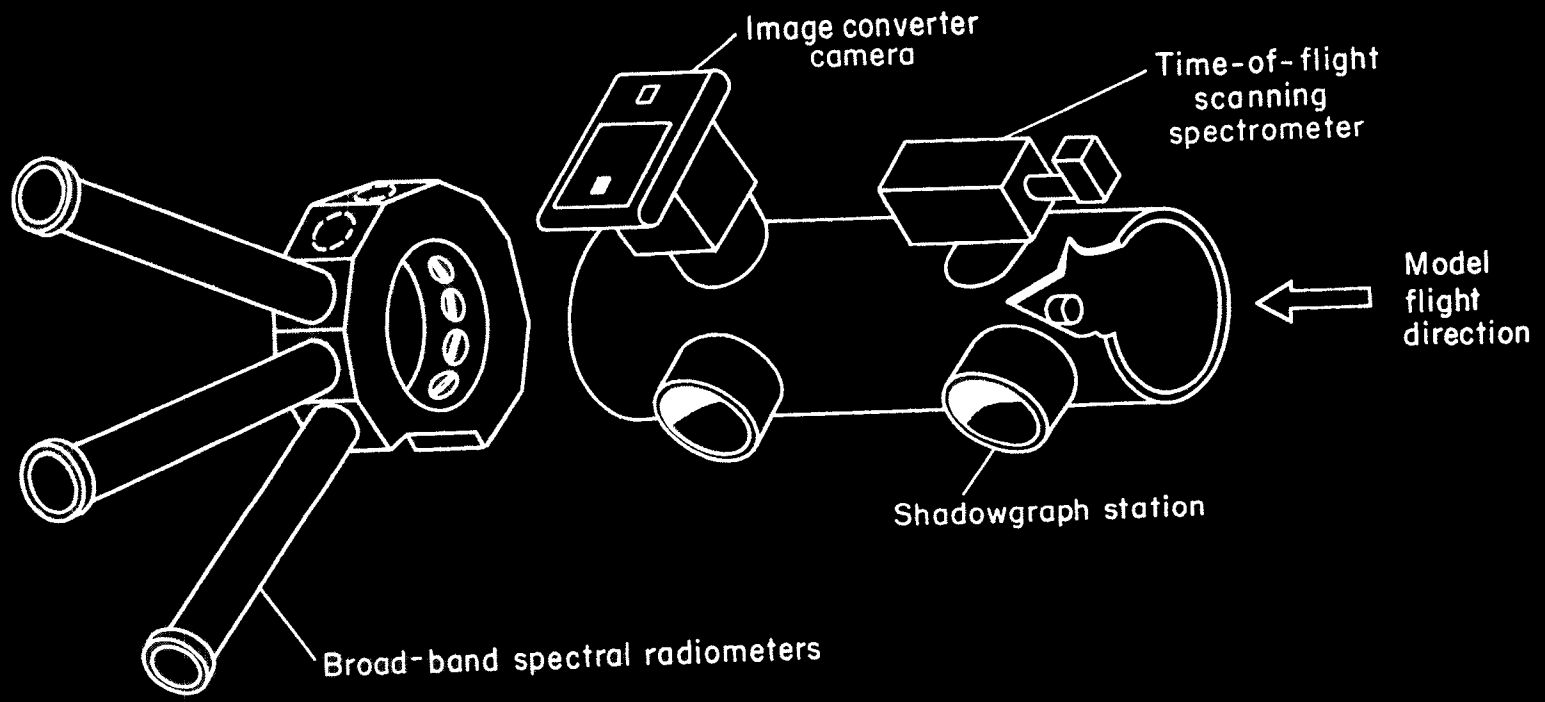

Fig. 1.- Sketch of test section.

NATIONAL AERONAUTICS AND SPACE ADMINISTRATION
AMES RESEARCH CENTER, MOFFETT FIELD, CALIFORNIA

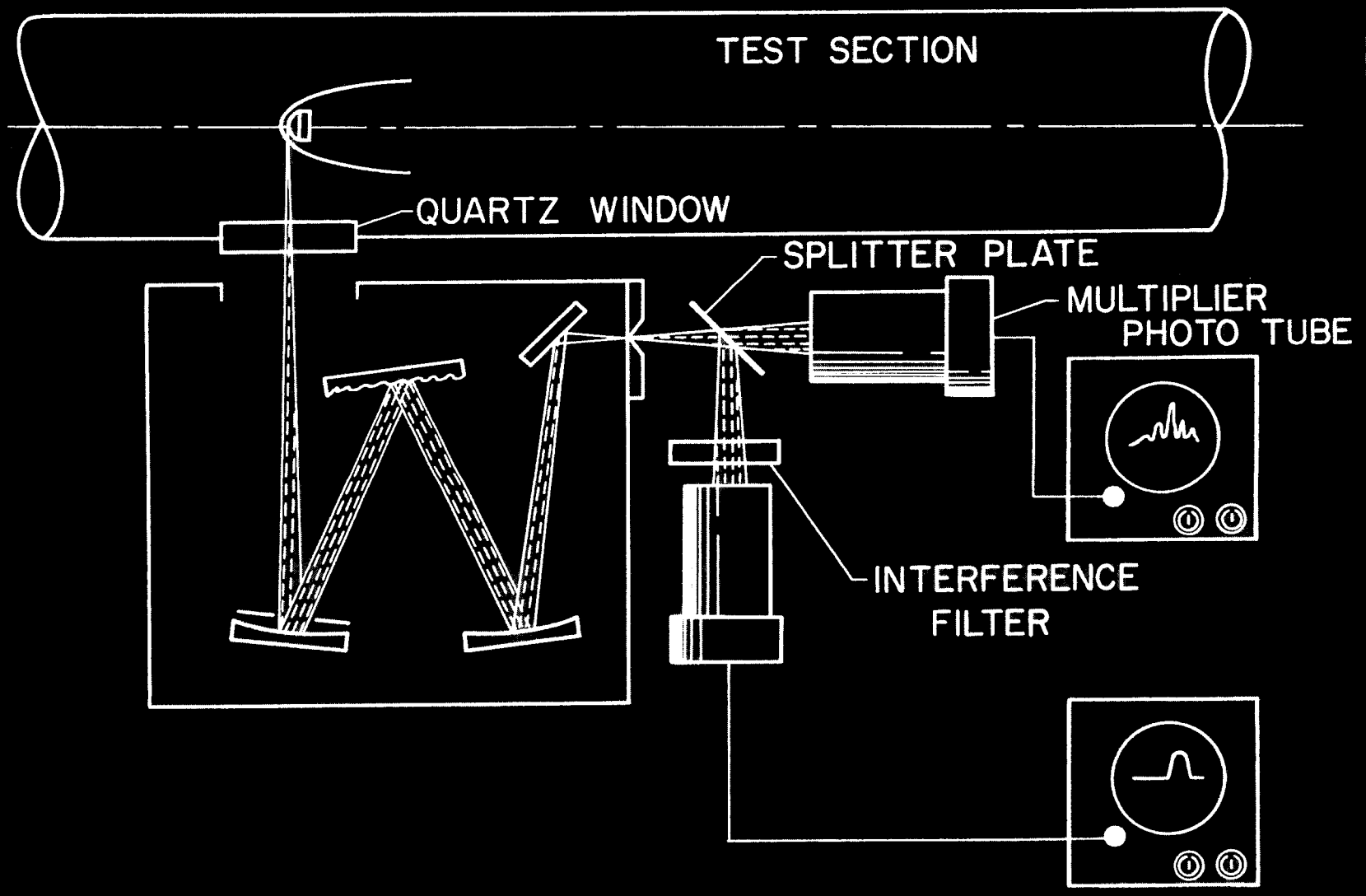

Fig. 2.- Time-of-flight scanning spectrometer.

NATIONAL AERONAUTICS AND SPACE ADMINISTRATION
AMES RESEARCH CENTER, MOFFETT FIELD, CALIFORNIA

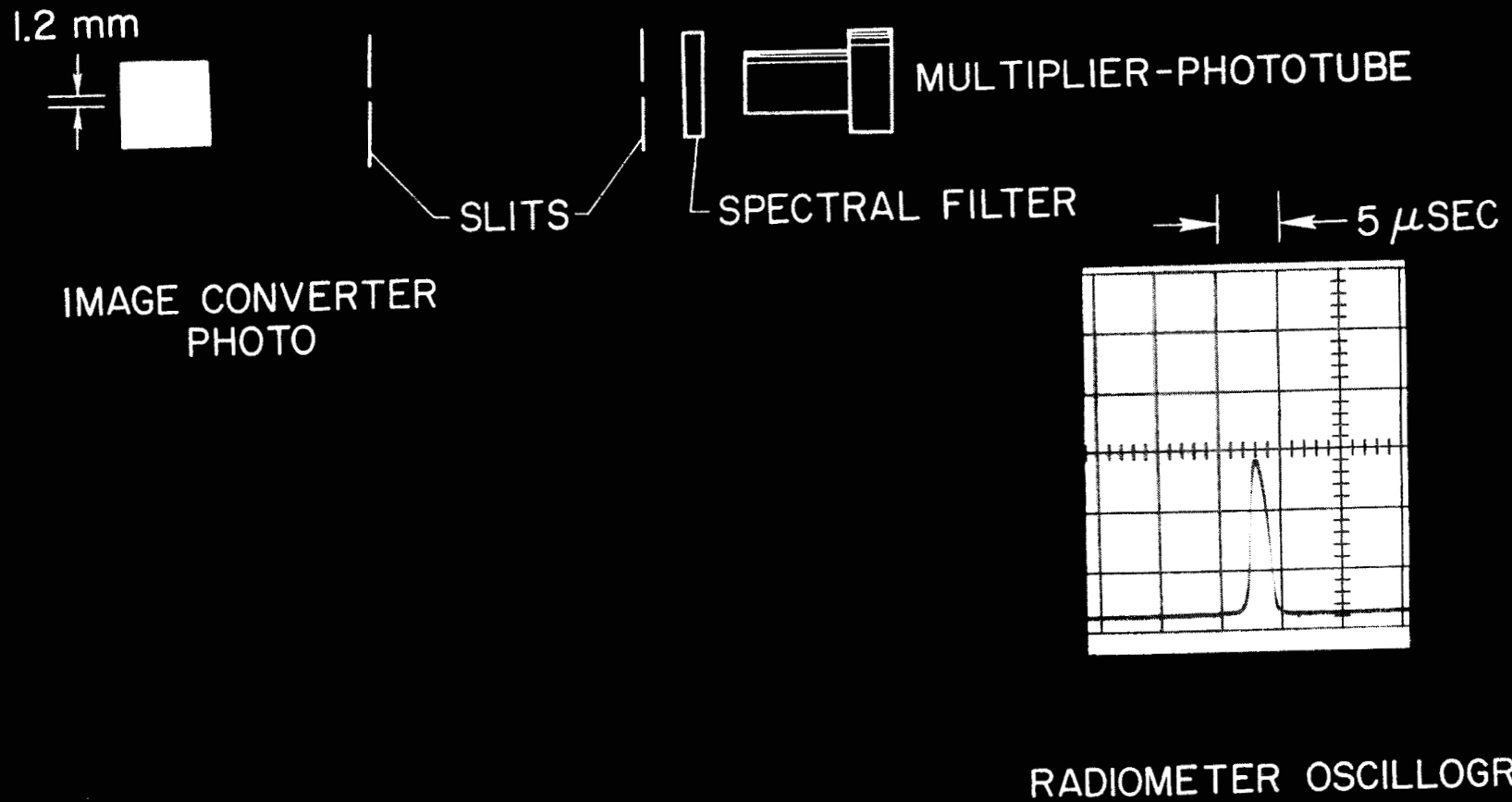

Fig. 3.- Image converter photograph and radiometer oscillogram showing slitlike appearance of shock layer.

NATIONAL AERONAUTICS AND SPACE ADMINISTRATION
AMES RESEARCH CENTER, MOFFETT FIELD, CALIFORNIA

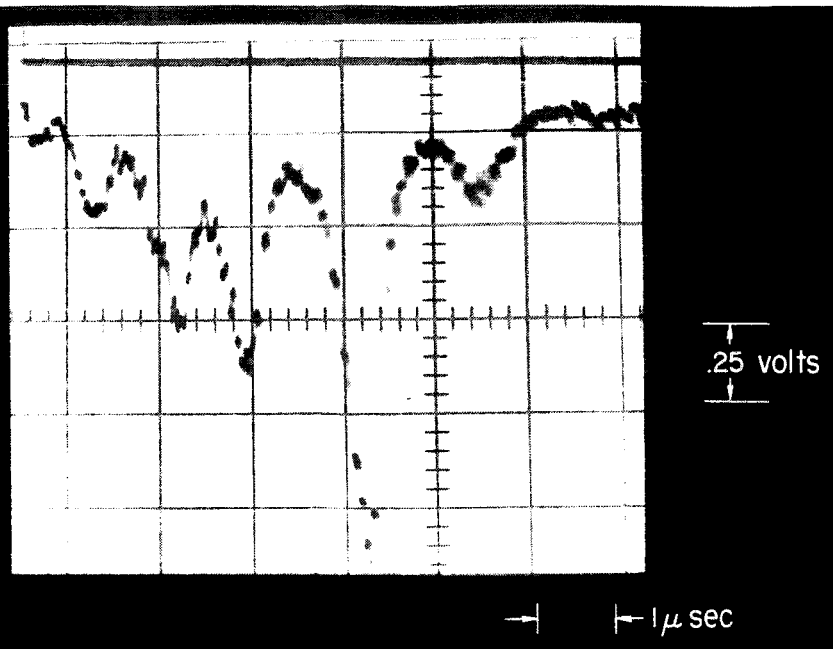

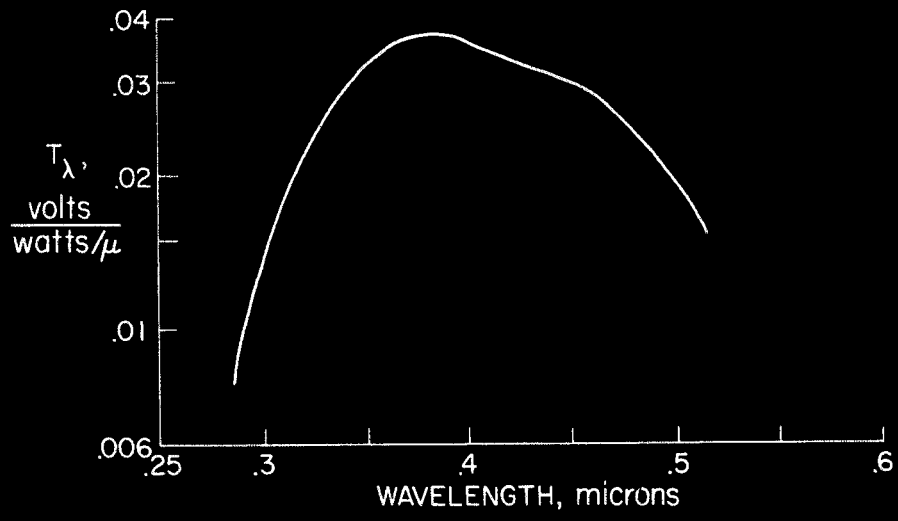

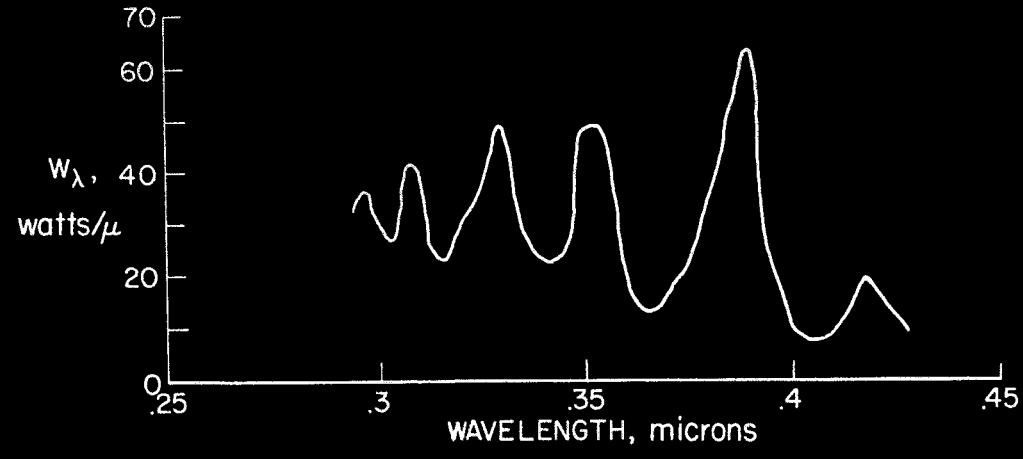

(a) Typical oscillogram from time-of-flight scanning spectrometer.
(b) Calibration curve of time-of-flight scanning spectrometer.
(c) Reduced experimental spectra.

Fig. 4.- Steps in determination of experimental spectra.

NATIONAL AERONAUTICS AND SPACE ADMINISTRATION
AMES RESEARCH CENTER, MOFFETT FIELD, CALIFORNIA

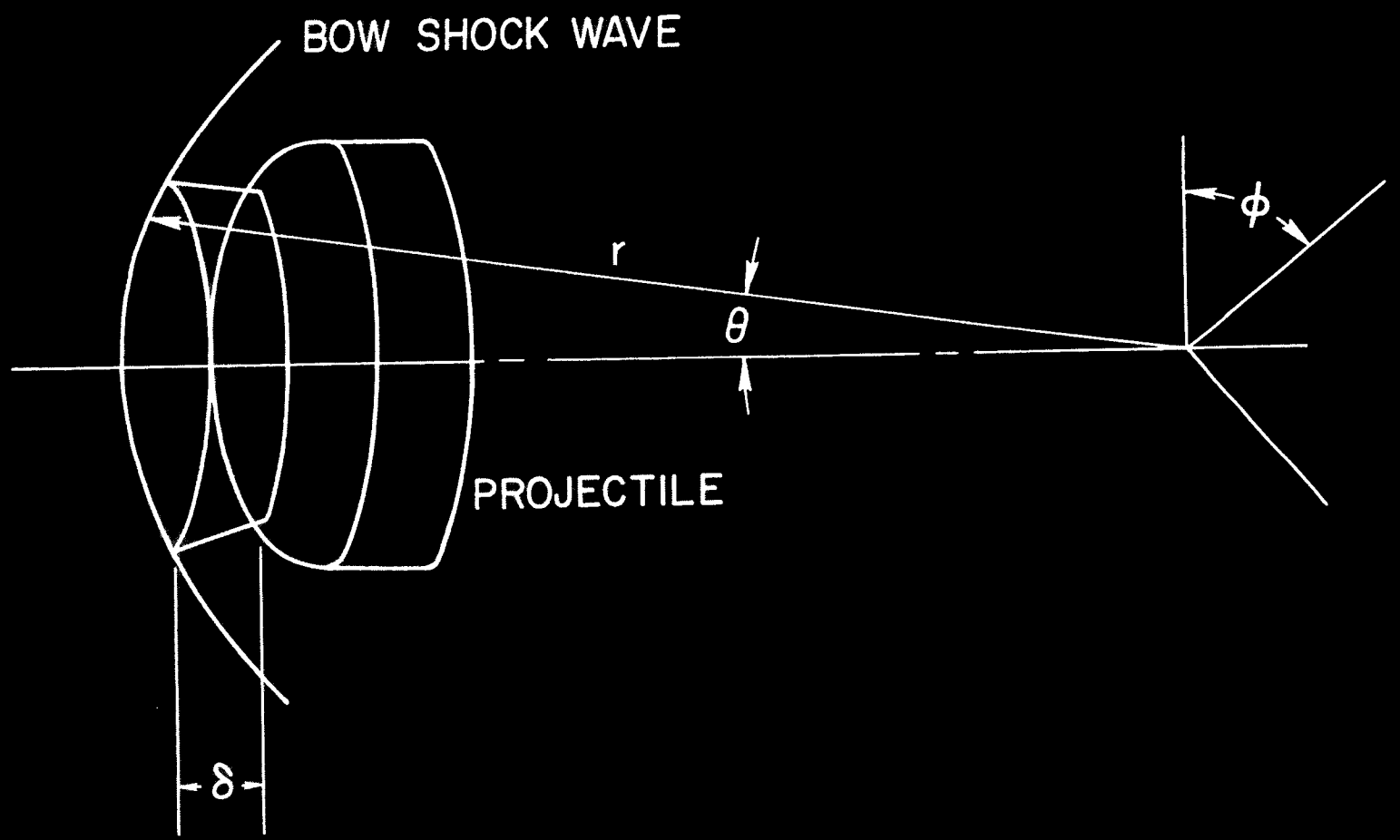

Fig. 5.- Coordinate system.

NATIONAL AERONAUTICS AND SPACE ADMINISTRATION
AMES RESEARCH CENTER, MOFFETT FIELD, CALIFORNIA

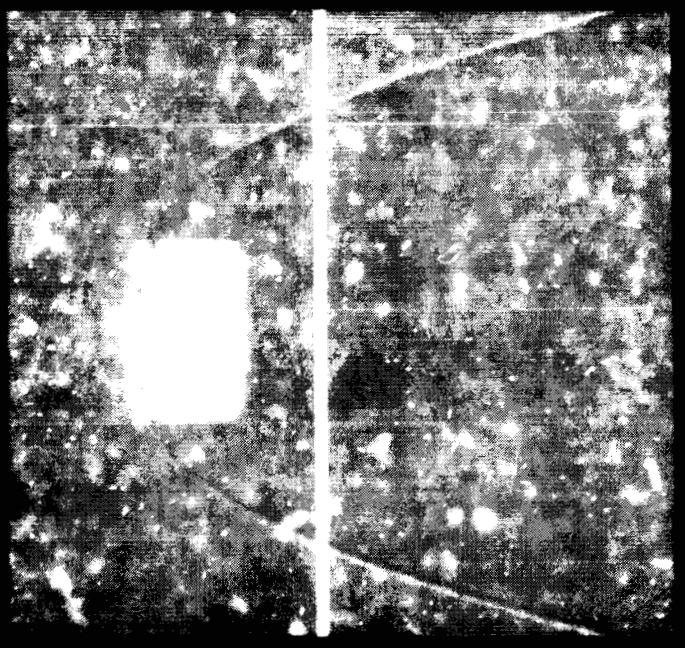

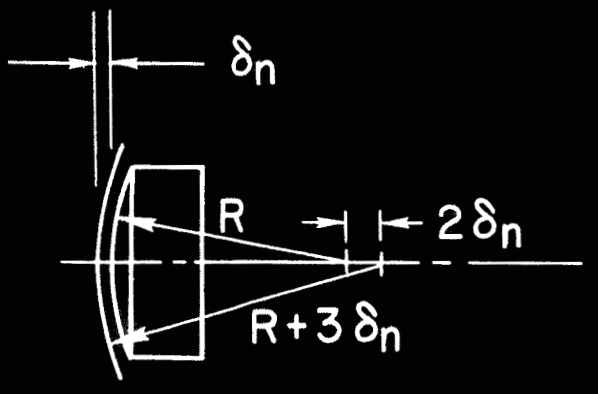

Fig. 6.- Typical shadowgraph of hypersonic projectile and assumed shock shape.

NATIONAL AERONAUTICS AND SPACE ADMINISTRATION
AMES RESEARCH CENTER, MOFFETT FIELD, CALIFORNIA

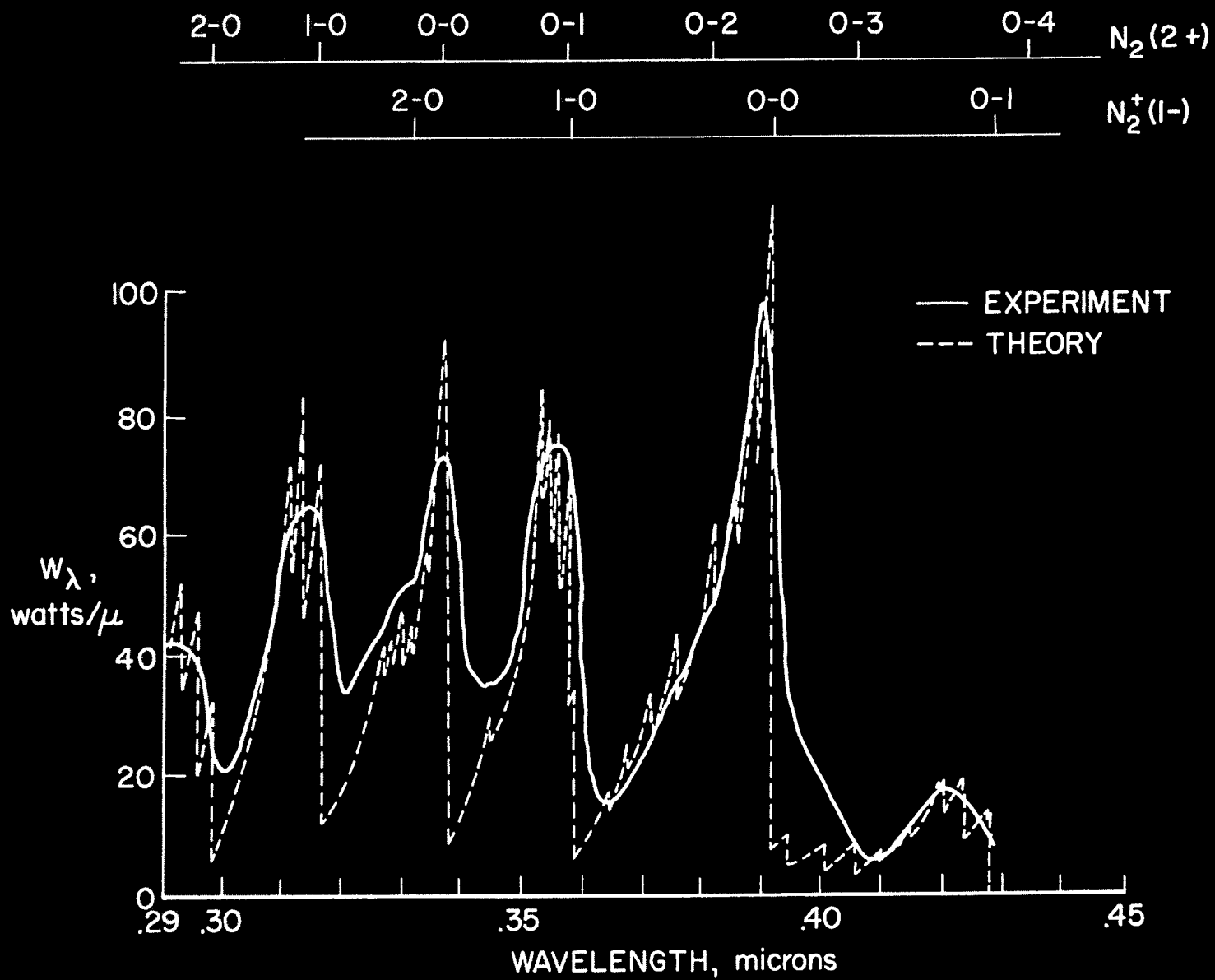

Fig. 7.- Comparison of calculated and experimental spectra.

NATIONAL AERONAUTICS AND SPACE ADMINISTRATION
AMES RESEARCH CENTER, MOFFETT FIELD, CALIFORNIA

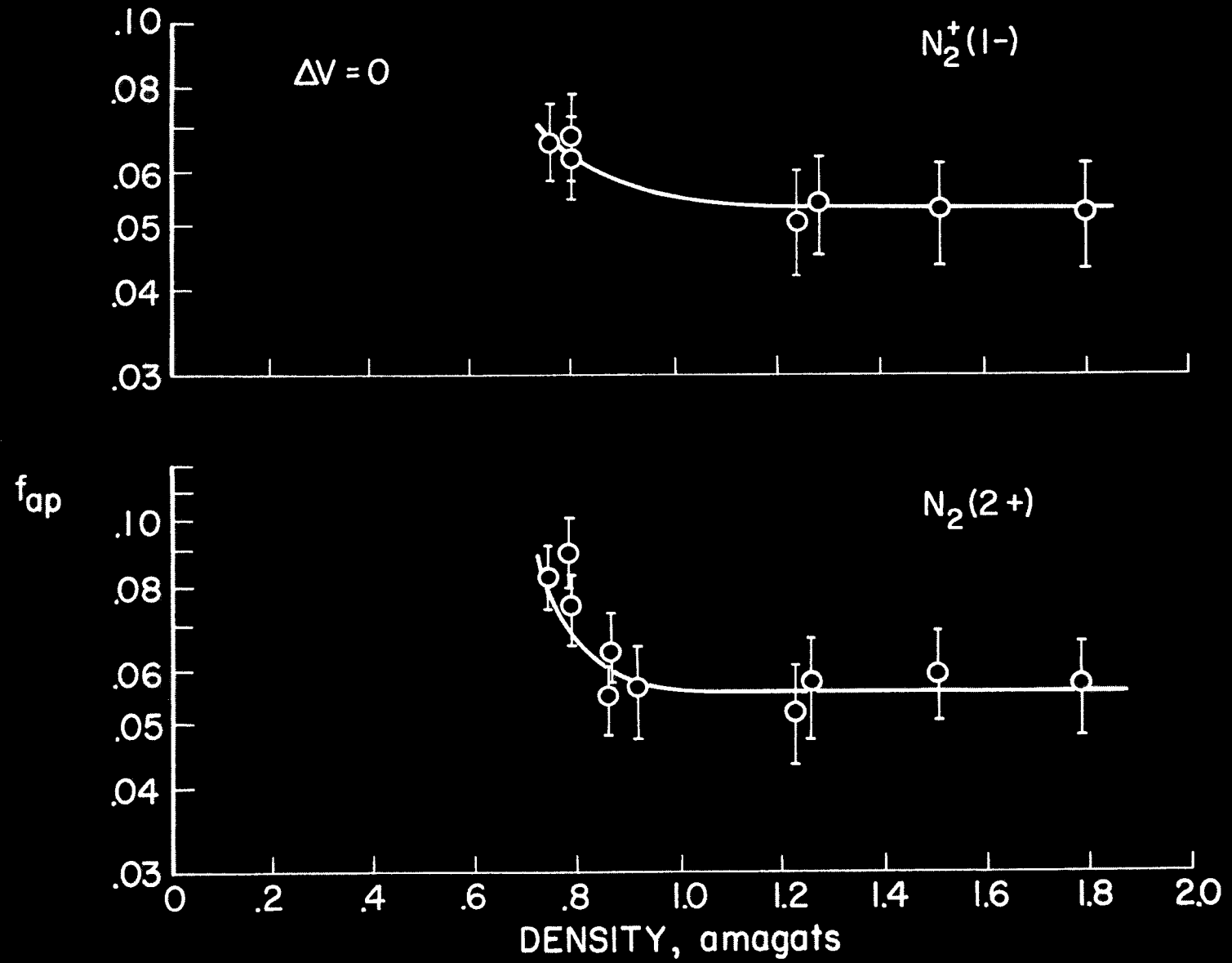

Fig. 8.- Variation of apparent f number with calculated equilibrium density behind bow shock.

NATIONAL AERONAUTICS AND SPACE ADMINISTRATION
AMES RESEARCH CENTER, MOFFETT FIELD, CALIFORNIA